

Advanced CFD-Based Coupled Computational Approach for Prediction of Complex Flight Behaviors

Jubaraj Sahu¹, Bradley Burchett², and Benjamin Gruenwald²

¹ Service Engineering, Belcamp, MD 21017

² U.S. Army Combat Capabilities Development Command - Army Research Laboratory,
Aberdeen Proving Ground, MD 21005

E-mail: jubaraj.sahu.ctr@army.mil

Abstract: This paper describes a computational study to understand aerodynamic and flight dynamic behaviors of a finned body with rear-fin (flap) control. Numerical simulations have been performed for this projectile with flap control using an advanced coupled computational fluid dynamics (CFD)/rigid body dynamics (RBD)/flight control system (FCS) technique. Special emphasis is on the FCS coupling for guided controlled flight simulations using an in-house MATLAB-based RBD/FCS code. An interface was developed for easy transfer of both the RBD state variables and the FCS variables of interest between the CFD flow solver and the RBD/FCS code. The coupled CFD/RBD/FCS capability has been exercised on a finned projectile with flap control and has been demonstrated using closed-loop pitch control and guided cross-range control maneuvers. Coupled results obtained show the resulting control flap deflection angles and their effect on the aerodynamics and flight dynamics of this projectile during the controlled maneuvers.

Keywords: Computational Fluid Dynamics, Coupled technique, Flight Controls.

1. Introduction

Improved computer technology and state-of-the-art numerical procedures now enable solutions to complex, three-dimensional problems associated with projectile and missile aerodynamics [1-3]. Detailed understanding of controlled flight behaviors is critical for enhanced vehicle maneuverability of these munitions. Advanced computational techniques are being developed to understand flight behaviors of both unguided and guided projectiles. One such technique couples computational fluid dynamics (CFD) and rigid body dynamics (RBD) for simultaneous prediction of unsteady aerodynamics and flight dynamics in an integrated manner [4]. The coupled approach is to capture static and dynamic aerodynamic behavior over short time durations with different motions. Performing coupled simulations in this manner allows for screening of situations where conventional aerodynamic models based on static wind tunnel or CFD techniques break down. These instances are encountered more often as wider classes of munitions (small-medium-large caliber) feature control inputs and the associated flow complexity such as interactions, unsteadiness, and high angle of attack. Thus, a major benefit of these coupled simulations is to mitigate risk of unanticipated flight behaviors during unguided and especially guided free-flight experiments. Also, in the traditional uncoupled approach, efforts are being directed at developing alternate CFD procedures such as angle of attack and Mach sweeps for rapid generation of aerodynamics for both simple and complex configurations at all speeds from subsonic to supersonic. In the present work, research has been focused on the

development and application of advanced a CFD-based coupled technique for accurate prediction of projectile aerodynamics and flight dynamics.

The advanced CFD capability used here solves the unsteady Navier-Stokes equations, incorporates unsteady boundary conditions and a special coupling procedure. This research is a big step forward in that it allows “virtual fly-out” of projectiles on the supercomputer, and it predicts the actual flight path of a projectile (flight dynamics) and all the associated unsteady free-flight aerodynamics in an integrated manner. In the coupled CFD/RBD procedure, the forces and moments are computed every CFD time step and transferred to a six degrees of freedom (6-DOF) module that computes the body’s response to the forces and moments. The response is converted into translational and rotational accelerations that are integrated to obtain translational and rotational velocities and integrated once more to obtain linear position and angular orientation. This method automatically takes into account flow interactions (e.g. canard-fin vortex interactions on a canard-controlled projectile) during the flight. It also yields a wealth of data unavailable in experimental methods, but it does involve highly intensive computer calculations requiring large computational resources. Flow fields, pressure distributions, forces and moments on various surfaces, and the complete twelve-state RBD history are available from the coupled solutions. The aerodynamic coefficients are then determined using regression and parameter estimation techniques.

Coupled CFD/RBD technique was first demonstrated on a finned projectile for the simulation of projectile free flight motion in a time accurate manner in 2008 [4]. This method has also recently been used for high-fidelity RBD and prescribed motion maneuvers of aircrafts and other flying vehicles [5-8]. This technique, also known as virtual fly-out method uses advanced CFD methods to characterize the unsteady aerodynamics at each instant in time during flight. Coupled CFD/RBD technique has already been demonstrated for various finned- and spin-stabilized projectiles [9-14] and validated in some of these cases. Recently, a flight control system (FCS) module [15] was added to the CFD/RBD technique resulting in a coupled capability for computation of unsteady aerodynamics and flight dynamics associated with guided control maneuvers [16, 17].

Current research efforts are focused on developing and implementing coupled CFD/RBD and CFD/RBD/FCS all using an in-house MATLAB-based 6DOF code. An advantage of using the in-house MATLAB code is its simplicity; it has just a RBD routine and an FCS routine. The big advantage comes from the flight control design itself; simple to complex (tracking, adaptive) FCS designs can be implemented and integrated easily into the coupled calculations for simulations of guided control maneuvers. The resulting coupled CFD/RBD/FCS technique can be used for open and closed loop control maneuvers where canards or fins are deflected in a desired fashion based on the control algorithm to provide control authority needed. The canard/fin deflection output vector of the flight control element is used to move the grid (locations and velocities) for the next CFD time step computation. CFD computes the aerodynamic forces/moments that dictates the projectile flight motion and subsequent controlled deflections subject to the control algorithm.

2. Computational Methodology

2.1 CFD Technique

The complete set of three-dimensional (3-D) time-dependent Navier-Stokes equations is solved in a time-asymptote manner to obtain converged steady-state solutions. A commercially available code, CFD++ [18,19], is used and the 3-D, time-dependent Reynolds-averaged Navier-Stokes (RANS) equations are solved using the following finite volume method:

$$\frac{\partial}{\partial t} \int_V \mathbf{W} dV + \oint [\mathbf{F} - \mathbf{G}] \cdot d\mathbf{A} = \int_V \mathbf{H} dV \quad (1)$$

where \mathbf{W} is the vector of conservative variables, \mathbf{F} and \mathbf{G} are the inviscid and viscous flux vectors, respectively, \mathbf{H} is the vector of source terms, V is the cell volume, and A is the surface area of the cell face.

Several techniques such as implicit scheme and relaxation are used to achieve faster convergence. Use of an implicit scheme circumvents the stringent stability limits suffered by their explicit

counterparts, and successive relaxation allows update of cells as information becomes available and thus aids convergence. Second-order discretization was used for the flow variables and the turbulent viscosity equation. The turbulence closure is based on topology-parameter-free formulations. A realizable two-equation $k-\epsilon$ turbulence model [20] was used for the computation of turbulent flows. These models are ideally suited to unstructured book-keeping and massively parallel processing due to their independence from constraints related to the placement of boundaries and/or zonal interfaces. The basic CFD solution technique described here is coupled with a RBD for simultaneous prediction of controlled and uncontrolled flights.

2.2 Coupled CFD/RBD/FCS Procedure

In the coupled CFD/RBD procedure, the forces and moments are computed every CFD time step and transferred to a six degrees of freedom (6DOF) module which computes the body's response to the forces and moments. The response is converted into translational and rotational accelerations that are integrated to obtain translational and rotational velocities and integrated once more to obtain linear position and angular orientation. This coupled technique provides both the unsteady aerodynamics and the flight dynamics in an integrated manner.

A time-accurate numerical approach is used in the coupled CFD/RBD simulations. This approach requires that the six-degrees-of-freedom (6DOF) RBD¹ be computed at each repetition of a flow solver. The CFD capability [18,19] used here solves the full Navier-Stokes equations and incorporates advanced boundary conditions and grid motion capabilities. For time-accurate simulations of coupled flights, a dual time-stepping procedure is generally used to achieve the desired time accuracy in the time-accurate solutions. The entire grid is moved to take into account the motion of the projectile. To account for rigid body dynamics, the grid point velocities were set as if the grid is attached to the rigid body with 6DOF.

Typically, the coupled solution procedure requires three steps. First, we begin with a computation performed in the "steady-state mode" with the grid velocities prescribed to account only for the translational motion component of the complete set of initial conditions. At the second step, we also impose the angular orientations from the initial conditions. At this stage, spin is normally added. In the present study, we are interested in pitching motions only; thus, spin is set to zero. Computations are performed in a time-accurate mode for a desired number of time-steps (500 to 1000). Converged solution from this second step provides the initial condition for the third step. In the third step, the remaining rotational velocity components (pitch and yaw) are added. The solution from the third step should correspond to the complete set of initial conditions that includes all translational and rotational velocity components and accounts for initial position and angular orientations. For simulations of controlled maneuvers (open-loop or closed-loop), a procedure which integrates flight control into the coupled CFD/RBD method is used.

2.3 MATLAB-Based 6DOF and Flight Controls

An inhouse RBD/FCS that is completely based on MATLAB has been developed and implemented in the coupled procedure. In addition to using the MATLAB environment, we added two significant enhancements to the existing in-house simulation framework.

First, continuous states from all subsystems (plant, actuator, control laws) are concatenated in one long system state vector and integrated simultaneously for more realistic continuous time simulation. The current implementation provides for up to 300 continuous states, however, expansion is easily facilitated by modifications to the .c based interface. To avoid difficulty compiling the MATLAB codes, we chose to make the MATLAB memory space completely volatile, requiring the state history to be stored entirely on the CFD++ side.

Second, actuator and control system state derivatives are sequestered to a subfunction in order to achieve modularity. Simulation users can provide their own actuator models and dynamic control systems without modifying the baseline CFD-RBD simulation engine.

The CFD++ simulation uses a twelve state input vector consisting of the vehicle position and mass center velocity in ground-fixed Cartesian coordinates, $\mathbf{X} = \{x \ y \ z\}$ and $\dot{\mathbf{X}} = \{\dot{x} \ \dot{y} \ \dot{z}\}$

respectively, the vehicle orientation expressed as the standard set of aircraft Euler angles ($\Theta = \{\phi \ \theta \ \psi\}$), and the three body-fixed angular rates ($\omega = \{p \ q \ r\}$). From these inputs it renders force/moment predictions in the ground-fixed frame.

The relationships between ground-fixed and body-fixed coordinates are illustrated in Figures 1 and 2.

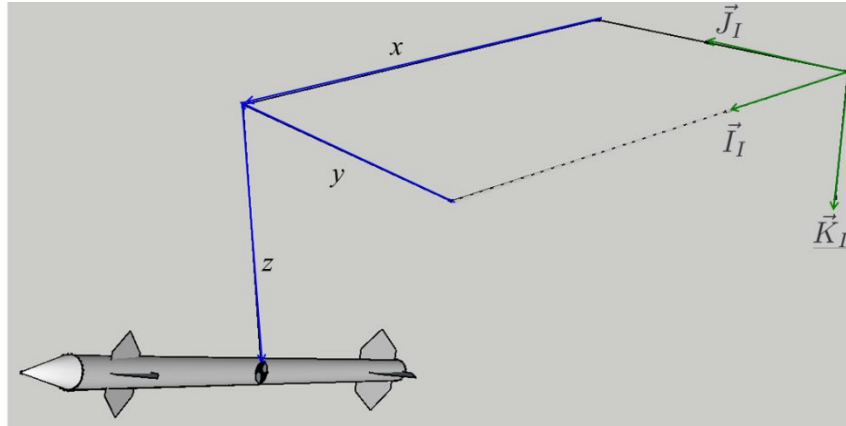


Figure 1: Ground-fixed Cartesian coordinates for projectile cg position defined

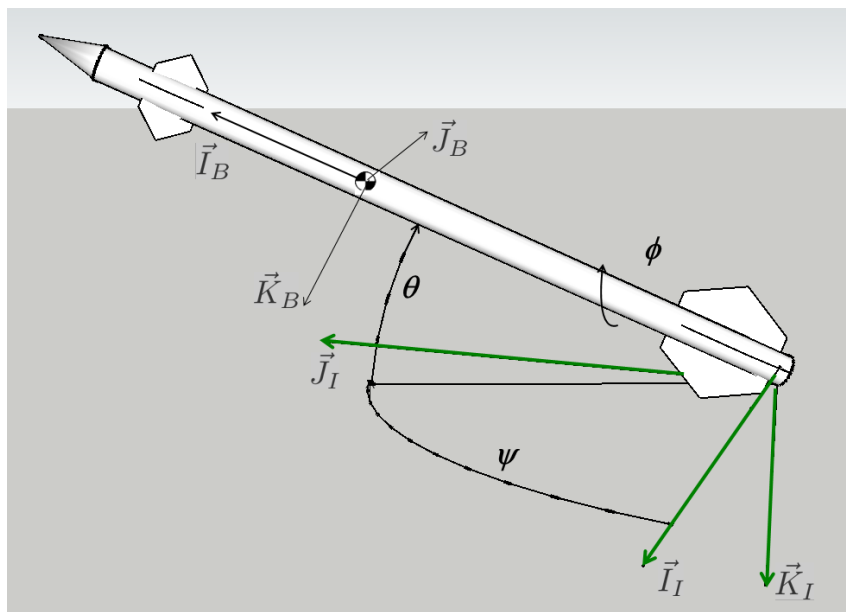


Figure 2: Standard Euler angles defined

Our six degree of freedom (6DOF) rigid body dynamic model uses a standard state vector consisting of the concatenation of: vehicle cg position in ground fixed Cartesian coordinates, $\mathbf{X} = \{x \ y \ z\}$, orientation as the customary set of Euler angles, $\Theta = \{\phi \ \theta \ \psi\}$, velocity in the body-fixed frame, $\mathbf{U} = \{u \ v \ w\}$, and body angular rates in the body frame, $\omega = \{p \ q \ r\}$. Thus, the overall state is $\zeta = \{\mathbf{X} \ \Theta \ \mathbf{U} \ \omega\}$.

Since the CFD uses ground-fixed velocity, forces, and moments, the first step in the RBD simulation is the transform these quantities into the body frame. Given

$$\mathbf{T}_{i2b} = \begin{bmatrix} c_\theta c_\psi & c_\theta s_\psi & -s_\theta \\ s_\phi s_\theta c_\psi - c_\phi s_\psi & s_\phi s_\theta s_\psi + c_\phi c_\psi & s_\phi c_\theta \\ c_\phi s_\theta c_\psi + s_\phi s_\psi & c_\phi s_\theta s_\psi - s_\phi c_\psi & c_\phi c_\theta \end{bmatrix}$$

the body fixed velocity vector is found as:

$$\mathbf{U} = \mathbf{T}_{i2b} \dot{\mathbf{X}} \quad (2)$$

the body fixed force vector $\mathbf{F}^{\text{RBD}} = \{X \ Y \ Z\}$ is given as:

$$\mathbf{F}^{\text{RBD}} = \mathbf{T}_{i2b} \mathbf{F}^{\text{CFD}} \quad (3)$$

and the body fixed moment vector $\mathbf{M}^{\text{RBD}} = \{l \ m \ n\}$ is given as:

$$\mathbf{M}^{\text{RBD}} = \mathbf{T}_{i2b} \mathbf{M}^{\text{CFD}} \quad (4)$$

The CFD force vector does not include gravity which is found as:

$$\vec{\mathbf{F}}_{grav} = \begin{Bmatrix} -S\theta \\ S\phi c\theta \\ c\phi c\theta \end{Bmatrix} mg = \mathbf{T}_{i2b} \begin{Bmatrix} 0 \\ 0 \\ mg \end{Bmatrix}$$

and simply added to render the total force on the projectile:

$$\mathbf{F}_{tot} = \mathbf{F}^{\text{RBD}} + \vec{\mathbf{F}}_{grav}$$

Once the required quantities are found in the body frame, the derivatives of the state vector follow a standard formulation:

$$\begin{Bmatrix} \dot{x} \\ \dot{y} \\ \dot{z} \end{Bmatrix} = \mathbf{T}_{i2b}^T \begin{Bmatrix} u \\ v \\ w \end{Bmatrix} \quad (5)$$

$$\begin{Bmatrix} \dot{\phi} \\ \dot{\theta} \\ \dot{\psi} \end{Bmatrix} = \mathbf{T}_{b2e} \begin{Bmatrix} p \\ q \\ r \end{Bmatrix} \quad (6)$$

$$\begin{Bmatrix} \dot{u} \\ \dot{v} \\ \dot{w} \end{Bmatrix} = \begin{Bmatrix} X/m \\ Y/m \\ Z/m \end{Bmatrix} - \mathbf{S} \begin{Bmatrix} u \\ v \\ w \end{Bmatrix} \quad (7)$$

$$\begin{Bmatrix} \dot{p} \\ \dot{q} \\ \dot{r} \end{Bmatrix} = [\mathbf{I}]^{-1} \begin{Bmatrix} l \\ m \\ n \end{Bmatrix} - \mathbf{S}[\mathbf{I}] \begin{Bmatrix} p \\ q \\ r \end{Bmatrix} \quad (8)$$

where

$$\mathbf{T}_{b2e} = \begin{bmatrix} 1 & s_\phi t_\theta & -c_\phi t_\theta \\ 0 & c_\phi & -s_\phi \\ 0 & s_\phi/c_\theta & c_\phi/c_\theta \end{bmatrix} \quad \mathbf{S} = \begin{bmatrix} 0 & -r & q \\ r & 0 & -p \\ -q & p & 0 \end{bmatrix}$$

and $[\mathbf{I}]$ is the three dimensional body-fixed inertia tensor.

The MATLAB RBD/FCS framework can facilitate the simulation of sophisticated control systems and has been used to demonstrate closed-loop model reference adaptive control. [21] For this work, we use a Linear Quadratic Regulator with reference inputs. A linearized model of the projectile dynamics is formed as

$$\dot{\mathbf{x}} = \mathbf{A}\mathbf{x} + \mathbf{B}\mathbf{u} \quad (9)$$

Where the state vector \mathbf{x} is defined in terms of the RBD states as $\mathbf{x} = [\phi \ p \ q \ r \ \dot{v} \ -\dot{w}]$ such that the last two states are lateral and normal acceleration in the body frame. The feedback control law is then given by

$$\mathbf{u} = -\mathbf{K}_1\mathbf{x} + \mathbf{K}_2\mathbf{r} \quad (10)$$

Where \mathbf{r} is the vector of commanded bank, lateral and normal acceleration ($\mathbf{r} = [\phi \ \dot{v} \ -\dot{w}]_{CMD}$).

\mathbf{K}_1 is found by solving the algebraic Riccati Eqn for \mathbf{P}

$$\mathbf{0} = \mathbf{P}\mathbf{A} + \mathbf{A}^T\mathbf{P} + \mathbf{Q} - \mathbf{P}\mathbf{B}\mathbf{R}^{-1}\mathbf{B}^T\mathbf{P} \quad (11)$$

then computing $\mathbf{K}_1 = \mathbf{R}^{-1}\mathbf{B}^T\mathbf{P}$. \mathbf{Q} and \mathbf{R} are user defined weighting matrices. The reference gain \mathbf{K}_2 is given by

$$\mathbf{K}_2 = -(\mathbf{E} \cdot (\mathbf{A} - \mathbf{B}\mathbf{K}_1)^{-1}\mathbf{B})^{-1}$$

Where \mathbf{E} is an output matrix that defines which states should track the reference commands. In the examples that follow

$$\mathbf{E} = \begin{bmatrix} \mathbf{1} & \mathbf{0} & \mathbf{0} & \mathbf{0} & \mathbf{0} & \mathbf{0} \\ \mathbf{0} & \mathbf{0} & \mathbf{0} & \mathbf{0} & \mathbf{1} & \mathbf{0} \\ \mathbf{0} & \mathbf{0} & \mathbf{0} & \mathbf{0} & \mathbf{0} & \mathbf{1} \end{bmatrix}$$

For the four-finned projectile, the commanded deflections are found by multiplying the virtual control \mathbf{u} by the control allocation matrix

$$\delta_{\text{CMD}} = \mathbf{C}_A \mathbf{u} \quad (12)$$

where

$$\mathbf{C}_A^T = \begin{bmatrix} -1 & -1 & -1 & -1 \\ -1 & 1 & 1 & -1 \\ -1 & -1 & 1 & 1 \end{bmatrix}$$

3. Computational Model and Mesh

The model geometry used represents a fin stabilized vehicle with four low-aspect-ratio fins symmetrically located around the body. It has a total length of 10 calibers. (Figure 3). It has an ogive nose that is approximately 3 calibers of the overall length of the body. This is followed by a cylindrical section and then ends with a 7° boattail beginning 0.5 caliber forward of the base. Also, this configuration has four independently actuated rear fin flaps for control. These movable flaps are approximately 0.75 calibers in length. The center of gravity is located at 5.6 calibers from the nose of the projectile. The projectile mass and other physical properties are listed in Table 1.

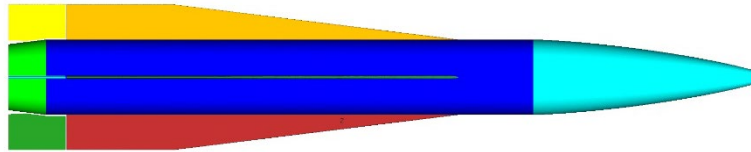


Fig. 3 Computational model

Table 1. Physical properties

Mass	19.718 kg
CG _x	588 mm from nose
CG _y , CG _z	on center line
I_{xx}	0.0301 kg-m ²
I_{yy}, I_{zz}	1.6664 kg-m ²

The computational mesh used was generated using multipurpose intelligent meshing environment (MIME) [22] an unstructured mesh generator developed by Metacomp Technologies, Inc. The total mesh size was approximately 65 M cells, consisting of triangular surface cells, with prism layers used along the surface and tetrahedral cells for the rest of the domain. The computational domain extended approximately 20 projectile lengths in all directions from the center of the projectile. The average cell size of the cylindrical density box (i.e., 2 cal. in radius, spanning 1 cal. forward to 5 cal. back of the projectile) was approximately 0.002 m. The first cell wall spacing of the prism layers was set to 3×10^{-7} m to ensure y^+ values of less than or equal to 1 along the surface of the projectile. The boundary layer spacing near the wall was selected so that a wall boundary condition that integrates all the way

to the wall could be used for turbulent flow calculations. A close-up view of the computational mesh near the body used for coupled simulations is presented in Fig. 4. An unstructured mesh was first obtained for the projectile w/o the movable flaps. Unstructured grids were then generated about each rear fin flap separately (Figure 5). The flap grids are then overset with the background projectile mesh to a Chimera overlapped mesh for the rear fin-controlled projectile. The advantage is that the individual flap grids were generated once and the Chimera procedure was then applied repeatedly as required during the flap motion without the need to generate the meshes at each time step for simulations with flap control.

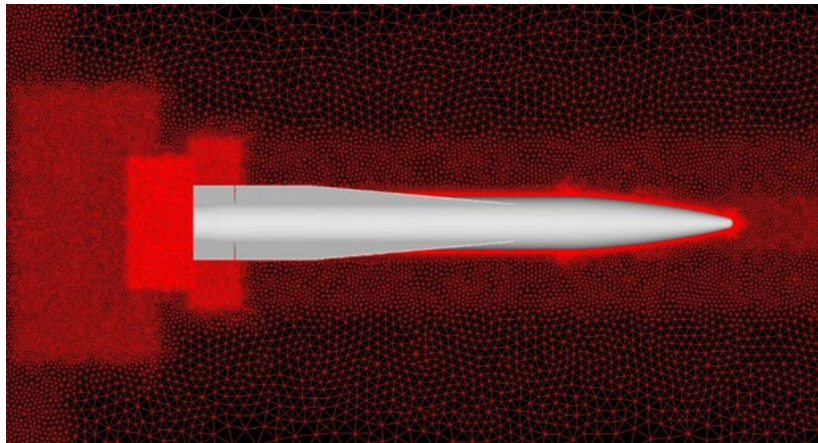


Fig. 4 Computational mesh expanded near the body

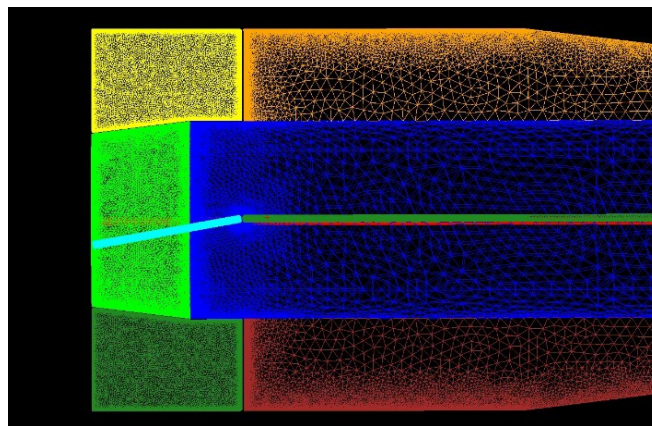


Fig. 5 Computational surface mesh showing one rear-fin flap deflected 10°.

4. Results

Coupled numerical computations were performed and virtual flyouts were carried out to accurately and efficiently predict the flow field and aerodynamic coefficients for a flap-controlled projectile configuration. All calculations were performed at initial Mach = 1.2 and 3.0 using atmospheric flight conditions. All computations were 3-D and performed in the pitch plane i.e. for roll orientation of 0° with fins in the “X” orientation. All numerical simulations of the virtual fly-outs have been carried out at DoD Defense Supercomputing Resource Centers (DSRC) using 384 - 512 processors on a Cray XC-40.

Since the calculations were all performed in the 6-DOF mode, only the first step in the coupled simulation which required a steady state result to be obtained at a given initial velocity corresponding

to only the translational motion of the projectile was used. The twelve variables are the inertial position components of the projectile mass center $\{x \ y \ z\}$, the standard Euler angles $\{\phi \ \theta \ \psi\}$, the components of the projectile mass center velocity $\{u \ v \ w\}$, and the body frame components of the projectile angular velocity vector $\{p \ q \ r\}$. Initially, the origin (0,0,0) was located at the CG of the projectile. The initial Euler angles were set to zero. Initial u was set to 408 and 1020 m/s for $M=1.2$ and $M=3$, respectively; initial v and w were set to zero. All initial rotational rates were set to zero in the present computations except for pitch rate, q .

Two specific scenarios that are highlighted in the present study are: (1) demonstration of closed-loop pitch control maneuvers, and (2) demonstration of bank-to-turn cross-range maneuvers. For each of these cases, an appropriate starting CFD solution was obtained before running the coupled CFD/RBD computation. The first step in the coupled simulation required a steady state result to be obtained at a given initial velocity corresponding to only the translational motion of the projectile. The converged steady-state solution was used as the starting condition for the time-accurate run in the uncoupled mode for 500 time steps until mean values of the forces and moments converged. The converged uncoupled solution formed the initial condition for the fully coupled CFD/RBD simulations along with the other initial conditions (e.g. pitch rate). Each simulation was run for approximately 1.0 second. A time step of 0.0005 sec was used in the time-accurate, coupled calculations. To complete each coupled simulation with TVC, approximately 50 hours of CPU time were required using 512 processors on a Cray XC40 located at the Navy DSRC.

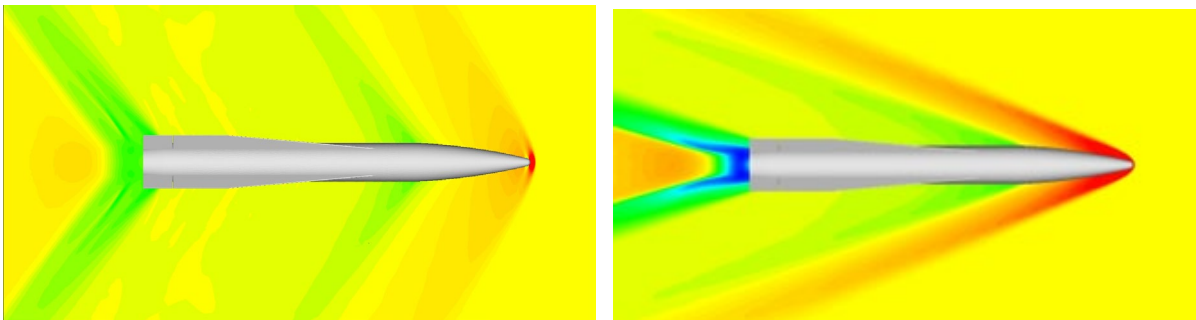


Figure 6. Computed pressure contours, $M=1.2$ (left), $M=3.0$ (right).

As part of this solution process, computed results have been obtained at initial speeds, $M = 1.2$ and 3.0 at zero degree angle of attack. Computed pressure contours for these two cases are shown in Figure 6. As expected, the flow field is symmetric for both cases. The bow shock wave in front of the nose, flow expansion at the ogive/cylinder junction and base, and recompression shock in near wake are all clearly evident. As Mach number increases from 1.2 to 3.0, one can see the bow shock getting stronger and the shock is closer to the body as is typical of supersonic flow.

As stated earlier, a variety of initial conditions were used for closed-loop and cross-range maneuvers and coupled simulations were performed for the finned projectile with rear flap control. Appropriate FCS designs or controllers were developed and used in the coupled CFD/RBD/FCS calculations for these maneuvers. Results obtained from the coupled calculations for these maneuvers are presented next.

4.1 Closed-loop Pitch Control Maneuvers

A first example considered is the pure pitch control of the finned projectile with flap control. All four control flaps were deflected up or down as needed during the closed-loop pitch control maneuver. The desired command is for the pitch rate to go to zero quickly. Again, coupled calculations have been performed at a high transonic velocity, $M=1.2$ and a supersonic velocity,

$M=3.0$. Initially, angle of attack, α was set to 0° for this projectile with flap control. Three initial pitch rates ($q = 0.3, 3.0,$ and 9.0 rad/s) were imposed. Coupled computational results were also obtained for corresponding uncontrolled cases for direct comparison.

The orientation of the projectile of course changes from one instant in time to another as the projectile flies down range. Coupled results of the pitch rate histories obtained at $M=1.2$ are shown in Figure 7. For all three controlled cases with various initial pitch rates, results show how quickly commanded zero pitch rate is reached. For the small $q=0.3$ rad/s, it is reached in less than 0.1 sec and for $q=3$ and 9 rad/s, in less than 0.2 sec. For the uncontrolled cases, we have free oscillatory pitching motions with the amplitude of pitching motion decreasing with time until eventually the mean pitch rate goes close to zero. Coupled results for the pitch control cases are very similar even at a higher $M=3.0$ (see Figure 8). For the uncontrolled cases at $M=3$, the frequency of pitch oscillations is larger than it is at $M=1.2$. However, for the controlled cases with flap control, the commanded zero pitch rate is achieved quickly again in less than 0.2sec.

Figure 9 shows the associated control flap deflections reaching a maximum of $1^\circ, 9^\circ,$ and 28° for the three pitch control maneuvers, respectively at $M=1.2$, and approximately $1^\circ, 11^\circ,$ and 28° for the three controlled pitch control maneuvers at $M=3.0$ (see Figure 10). Computed Euler pitch angles obtained from the pitch control maneuvers are shown in Figures 11a and b respectively for $M=1.2$ and 3.0 . The pitch angle, and hence, the angle of attack are held below 9° .

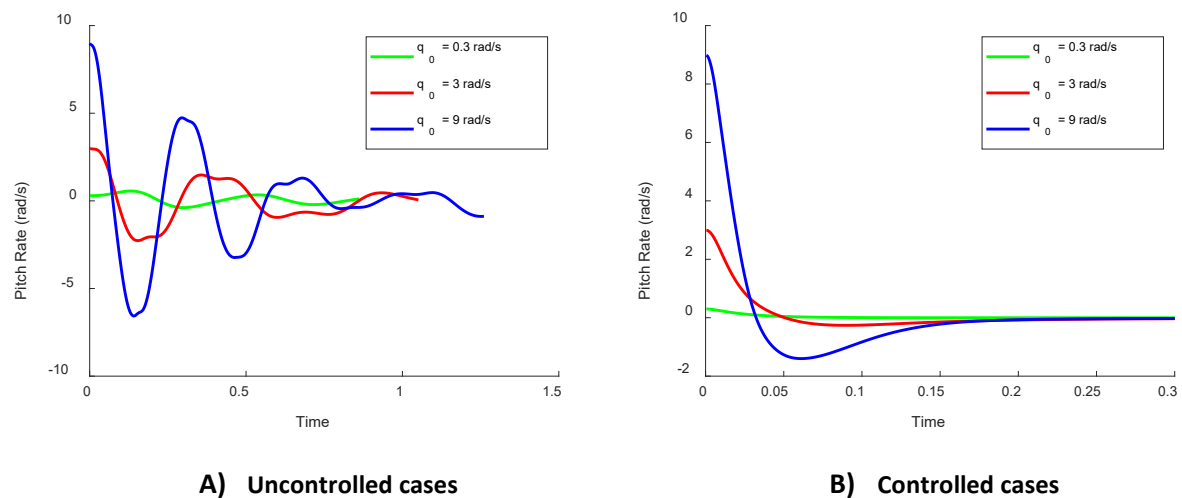


Figure 7. Comparison of angular rates (uncontrolled and controlled), initial $M=1.2$.

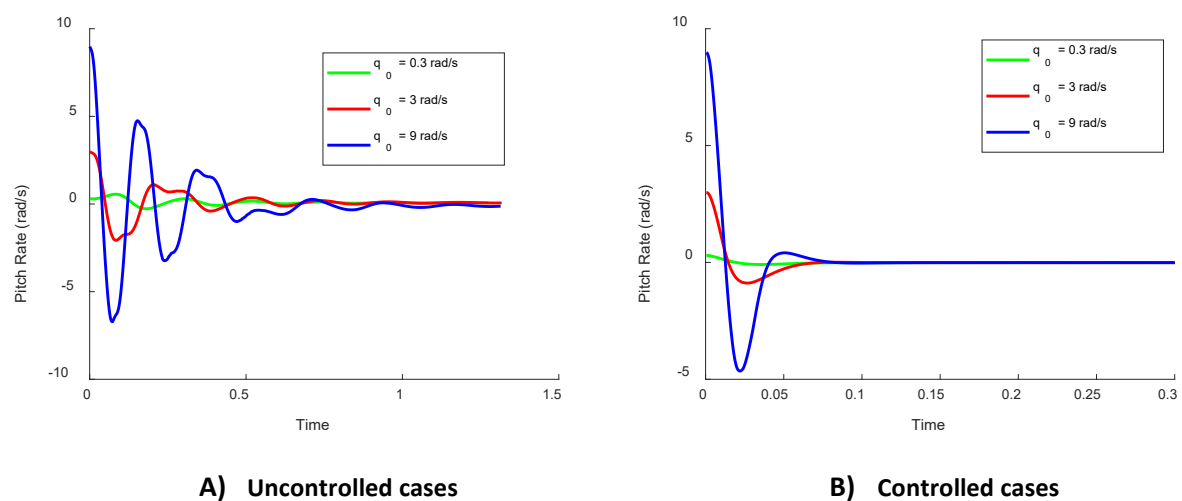
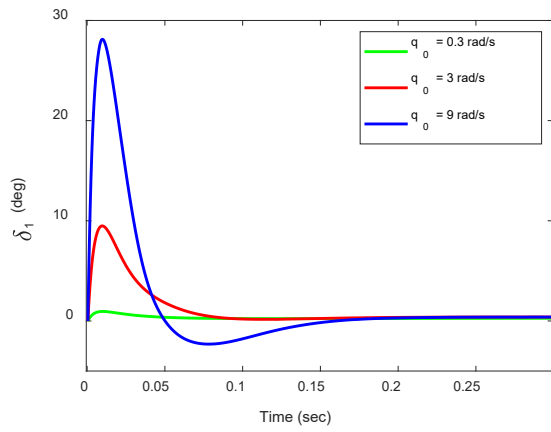
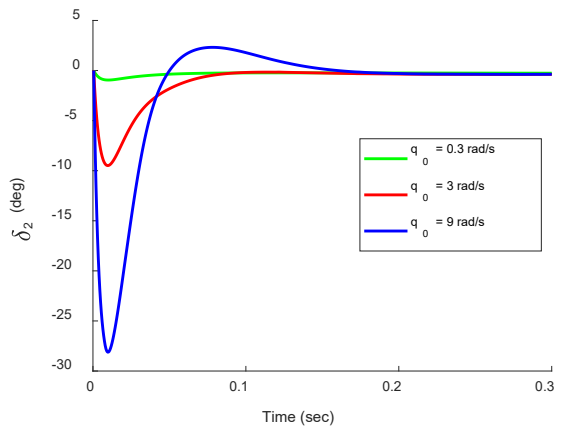


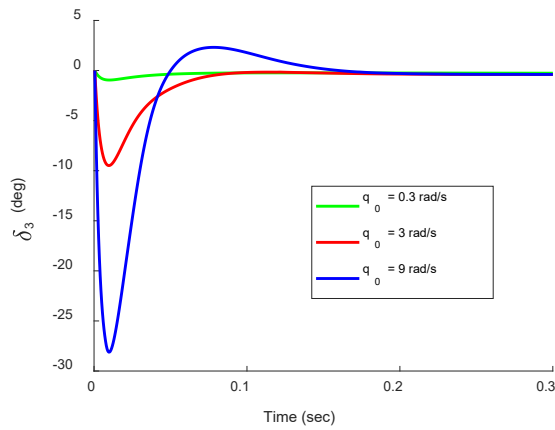
Figure 8. Comparison of angular rates (uncontrolled and controlled), initial $M=3.0$.



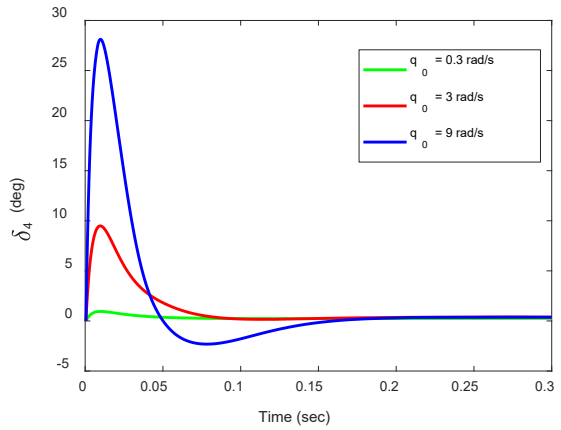
A) Flap 1 response



B) Flap 2 response

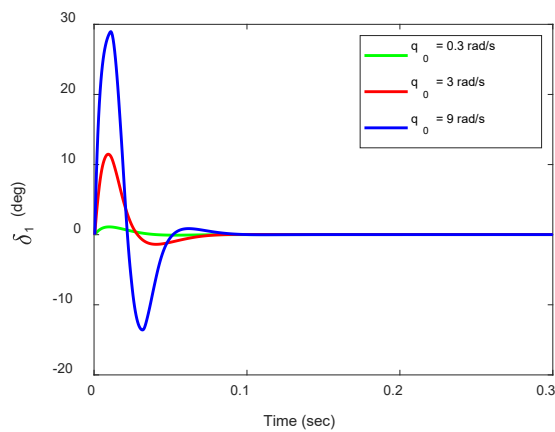


C) Flap 3 response

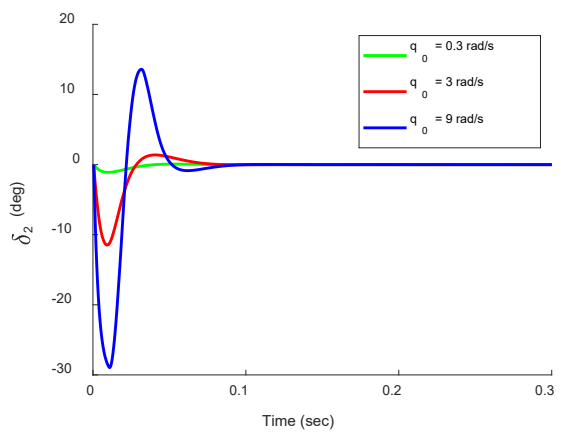


D) Flap 4 response

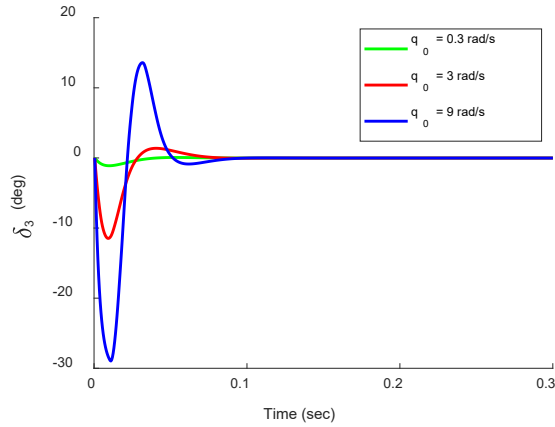
Figure 9. Control flap deflection angles for controlled cases, initial M=1.2.



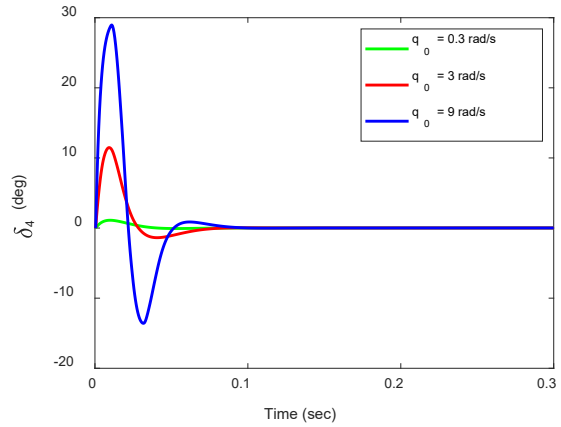
A) Flap 1 response



B) Flap 2 response

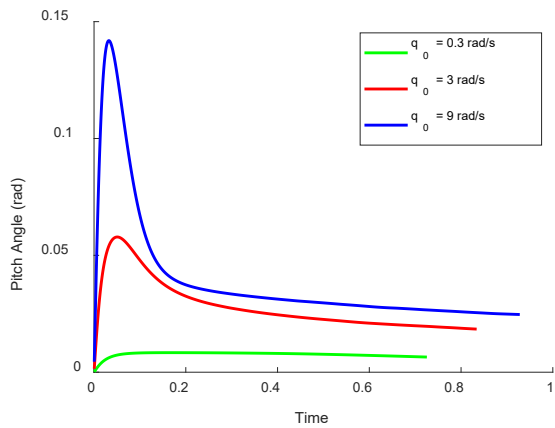


C) Flap 3 response

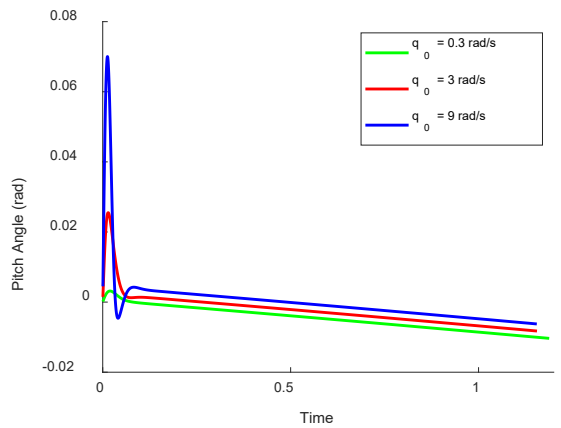


D) Flap 4 response

Figure 10. Control flap deflection angles for controlled cases, initial $M=3.0$.



A) Initial $M=1.2$.



B) Initial $M=3.0$.

Figure 11. Euler pitch angle for controlled cases

4.2 Bank-to-turn Cross-Range Maneuvers

We designed a bank-to-turn scenario to demonstrate the full capabilities of the simulation with a realistic multi-axis maneuver. Starting from level flight at Mach 1.2 or Mach 3, the projectile banks right to 75.5 degrees, then increases normal load factor to 4g. This should result in a level coordinated turn as shown in Figure 12. The reference commands and actual responses are shown in Figs 12a and b. The missile rolls rapidly to the commanded bank with small overshoot, settling well before the normal acceleration command is initiated. At $\frac{1}{4}$ second, the normal acceleration command steps up to 4g. The system responds quickly, however the underlying control design is based on an inaccurate model of the system gain, so the actual acceleration settles to a value much larger than that commanded.

Several other state variables are plotted in Figs 12c, d, e, and f. Fig 12c contains the crossrange and altitude responses, Note that crossrange increases during the maneuver in a quadratic fashion as

expected. Constant lateral acceleration commands at different airspeeds render roughly the same crossrange response despite the large difference in airspeed as crossrange is merely lateral acceleration integrated twice with respect to time. The high-speed case would trace a larger radius circle during the maneuver, but the crossrange achieved over 1.5 seconds is about the same. Altitude remains essentially constant in both cases, indicating level flight. Fig. 12d shows the yaw angle response. It begins to ramp up quickly at $\frac{1}{4}$ second, then continues to ramp up gradually once the turn is established. Note that the turn rate is much faster for $M=1.2$, as this is inversely proportional to airspeed for constant bank. Even more striking is the time rate of change of crossrange shown in Fig 12e. This value ramps up linearly, indicating that constant acceleration in the lateral direction has been achieved. Finally, Fig 12f shows the pitch angle. Note that the axis scaling is an order of magnitude smaller than that for yaw. Thus, level flight has been achieved.

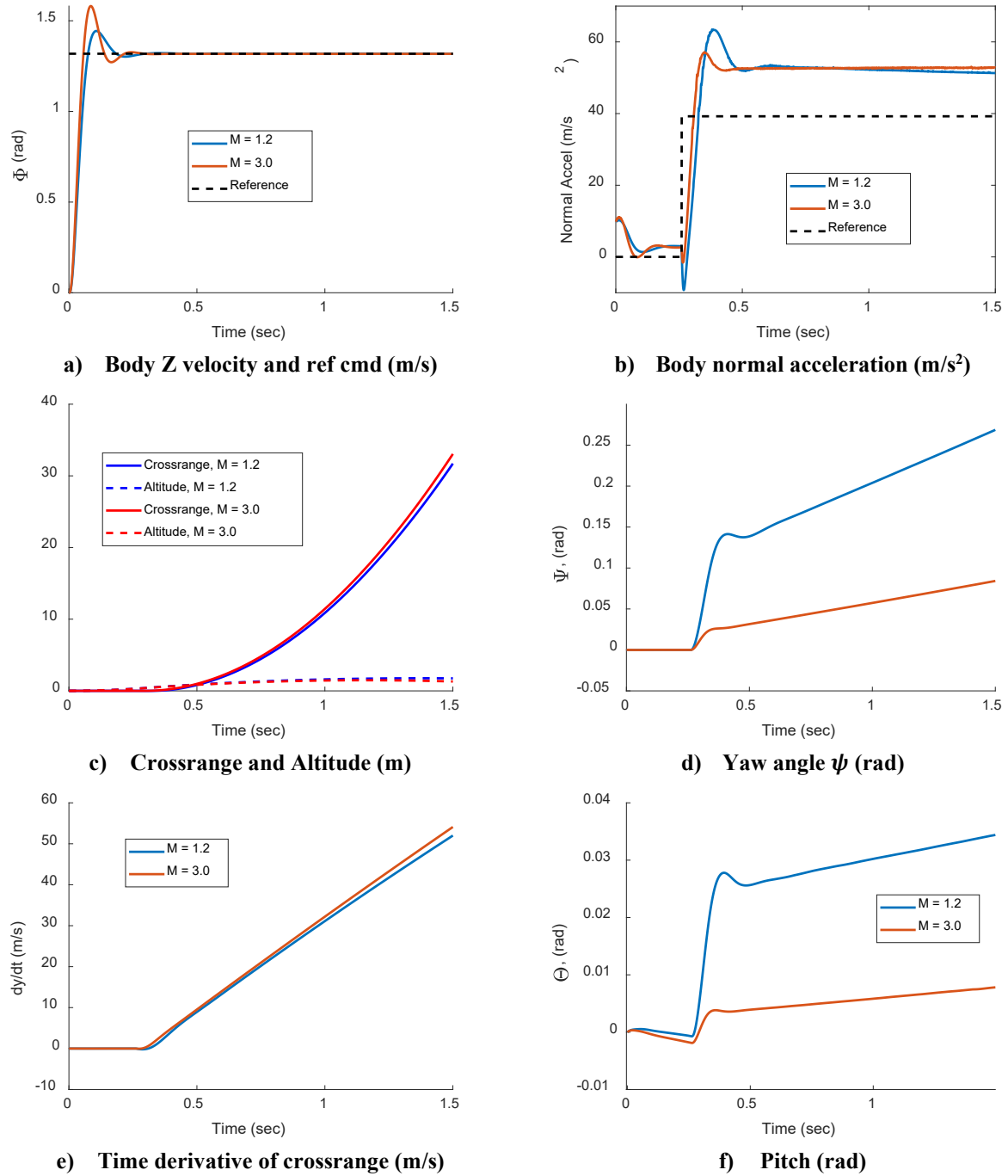


Fig. 12 Subset of state history, baseline LQR controller bank-to-turn scenario flow at $M=1.2$ and $M=3.0$.

5. CONCLUSIONS

Advanced numerical simulations were performed on a finned body with flap control using a new MATLAB-based coupled CFD/RBD/FCS procedure and a three-dimensional unsteady unstructured Navier-Stokes computational technique. In the coupled calculations, unsteady aerodynamics and flight dynamics were computed simultaneously and the response of the vehicle was determined at both $M=1.2$ and 3.0 for two maneuver scenarios.

The first scenario was used to demonstrate the new coupled simulations for closed-loop maneuvers with flap control and compare these results with corresponding uncontrolled cases. Coupled calculation automatically captures the relevant unsteady aerodynamics associated with flap control. Rear flaps were deflected to provide the control authority needed to bring the pitch rate to zero. In each closed-loop maneuver starting with various initial pitch rates, desired zero pitch rate was achieved quickly in less than 0.2sec. The bank-to-turn cross-range maneuver scenarios demonstrated increasing complexity in the coupled simulations and flight control designs. These bank-to-turn maneuvers resulted in cross-range of over 30m in less than 1.5s for both $M=1.2$ and 3 cases. Each of the control scenarios showed both the expanded capabilities of the simulation and the ease with which the user can import highly complex control systems using MATLAB.

This study is a significant step forward in the development of a coupled capability for prediction of flight behaviors of complex munitions for closed-loop control and guided control maneuvers. Further research is needed to implement, test, and validate highly complex tacking and adaptive flight control designs using coupled CFD/RBD/FCS technique and extend its application to complex maneuvers involving non-linear high angle of attack flights.

References

- [1] Sahu, J., "Numerical Computations of Dynamic Derivatives of a Finned Projectile using a Time-Accurate CFD Method," AIAA Paper 2007-6581, August 2007.
- [2] Siltou, S., "Navier-Stokes Computations for a Spinning Projectile from Subsonic to Supersonic Speeds," Journal of Spacecraft and Rockets, Vol. 42, No 2, pp 223-231, 2005.
- [3] DeSpirito, J., "Lateral Jet Interaction on a Finned Projectile in Supersonic Flow," AIAA 50th Aerospace Sciences Meeting, Nashville, TN, January 2012.
- [4] Sahu, J., "Time-Accurate Numerical Prediction of Free-Flight Aerodynamics of a Finned Projectile", AIAA Journal of Spacecraft and Rockets, Vol. 45, No 5, pp 946-954, 2008.
- [5] D. Guo et al., "Time-Accurate Simulation of Longitudinal Flight Mechanics with Control by CFD/RBD Coupling", Applied Mechanics and Materials, Vols. 226-228, pp. 788-792, Nov 2012.
- [6] Franze, M., "Comparison of a Closed-Loop Control by Means of High-Fidelity and Low-Fidelity Coupled CFD/RBD Computations", European Aeronautics and Aerospace Science Conf., 2017.
- [7] Dean, J.P., Clifton, J.D., Bodkin, D.J., and Ratcliff, C.J., "High Resolution CFD Simulations of Maneuvering Aircraft Using the CREATE-AV/Kestrel Solver", AIAA-Paper 2011-1109, 49th AIAA Aerospace Sciences Meeting, Orlando, Florida, 4 - 7 January 2011.
- [8] Ernst, Z., Drosendahl, M., Robertson, B., and Mavris, D., "Development of a Trajectory-Centric CFD-RBD Framework for Advanced Multidisciplinary/Multiphysics Simulation", AIAA SciTech Forum, January 3-7, 2022, San Diego, California, doi: 10.2514/6.2022-1793.
- [9] Sahu, J., "Virtual Fly-Out Simulations of a Spinning Projectile from Subsonic to Supersonic Speeds," AIAA Applied Aerodynamics Meeting, Honolulu, HI, June 2011.
- [10] Costello, M.; Sahu, J. Using Computational Fluid Dynamic/Rigid Body Dynamic Results to Generate Aerodynamic Models for Projectile Flight Simulation. Journal of Aerospace Engineering 2008, 22 (G7), 1067–079.
- [11] Sahu, J. and Fresconi, F., "Flight Behaviors of a Complex Projectile using a Coupled CFD-based Simulation Technique: Free Motion," AIAA-2015-2585, June 2015.
- [12] pSahu, J., Fresconi, F., and Heavey, K., "Unsteady Aerodynamics of a Finned Projectile at a Supersonic Speed with Jet Interaction," AIAA Paper 2014-3024, Atlanta, GA, June 2014.
- [13] Sahu, J., Costello, M, and Montalvo, C., "Development and Application of Multidisciplinary Computational Techniques for Projectile Aerodynamics", Paper No. ICCFD7-4504, 7th International Conference on Computational Fluid Dynamics, Big Island, HI, July 2012.
- [14] Sahu, J. and Fresconi, F. " Flight Behaviors of a Complex Projectile using a Coupled CFD-based Simulation Technique: Free Motion," AIAA Paper 2015-2585, Aviation Forum, Dallas, TX, June 2015.

- [15] Sahu, J., Fresconi, F., and Heavey, K. "Control Performance, Aerodynamic Modeling and Validation of Coupled Simulation Techniques for Guided Projectile Roll Dynamics," Paper 2014-2191, AIAA Aviation 2014 Forum, Atlanta, GA, June 2014.
- [16] Sahu, J. and Fresconi, F. " Flight Behaviors of a Complex Projectile using a Coupled CFD-based Simulation Technique: Open-loop Control," AIAA 2016-2025, SciTech Forum and Exposition, San Diego, CA, January 2016.
- [17] Sahu, J and Fresconi, F., "Flight Behaviors of a Complex Projectile using a Coupled CFD-based Simulation Technique: Closed-loop Control", AIAA 2016-4332, Aviation Forum, Wash D.C., June 2016.
- [18] Peroomian, O., Chakravarthy, S., and Goldberg, U. "A 'Grid-Transparent' Methodology for CFD." AIAA Paper 97-07245, 1997.
- [19] Peroomian, O., Chakravarthy, S., Palaniswamy, S., and Goldberg, U., "Convergence Acceleration for Unified-Grid Formulation Using Preconditioned Implicit Relaxation." AIAA Paper 98-0116.
- [20] Goldberg, U., Peroomian, O., and Chakravarthy, S., "A Wall-Distance-Free K-E Model with Enhanced Near-Wall Treatment." ASME Journal of Fluids Eng., Vol. 120, pp. 457-462, 1998.
- [21] Sahu, J., Gruenwald, B., and Burchett, B. "Adaptive Control Validation using a MATLAB based CFD / RBD Coupled Simulation", Army Research Laboratory (US); 2022 Apr. Report No.: ARL-TR-9433.
- [22] Metacomp Technologies, MIME user's manual, Agoura Hills, CA, 2012.